

Application of Computational Fluid Dynamics Simulations to the Analysis of Bank Effects in Restricted Waters

D. C. Lo, Dong-Taur Su, Jan-Ming Chen

(National Kaohsiung Marine University, Kaohsiung, Taiwan)

(E-mail: loderg@mail.nkmu.edu.tw)

It is well known that vessels operating in the vicinity of a lateral bank experience a significant yaw moment and sway force. This *bank effect* has a major impact on the manoeuvring properties of the vessel and must therefore be properly understood to ensure the safe passage of the vessel through the restricted waterway. Accordingly, this study performs a series of simulations using commercial FLOW-3D[®] computational fluid dynamics (CFD) software and the KRISO 3600 TEU container ship model to examine the effects of the vessel speed and distance to bank on the magnitude and time-based variation of the yaw angle and sway force. The results show that for a given vessel speed, the yaw angle and sway force increase as the distance to bank reduces, while for a given distance between the ship and the bank, the yaw angle and sway force increase with an increasing vessel speed. In addition, it is shown that even when a vessel advances at a very low speed, it experiences a significant bank effect when operating in close vicinity to the bank. Overall, the results presented in this study confirm the feasibility of the CFD modelling approach as a means of obtaining detailed insights into the bank effect without the need for time-consuming and expensive ship trials.

KEY WORDS

1. Computational Fluid Dynamics (CFD). 2. Bank Effects. 3. Sway Force. 4. Yaw Moment.

1. INTRODUCTION. When operating in restricted water and forced to deviate from the centre of the channel under vessel meeting and passing conditions, a ship inevitably approaches the bank and thus an asymmetric flow pattern is produced which generates a pressure difference between the port and starboard sides of the vessel. Generally speaking, a suction effect is induced toward the stern of the vessel, while a cushioning effect is induced at the bow. Thus, as shown in Figure 1, the vessel experiences a positive yaw moment, N_b , which pushes the bow toward the centre of the channel and a lateral sway force, Y_b , which is directed principally toward the nearest bank. This phenomenon is known as the bank effect and depends on many parameters, including the vessel speed, the distance to bank, the propeller speed, the water depth, the shape of the bank, and so forth. The bank effect has a significant impact on the manoeuvring characteristics of the vessel and must therefore be taken into account when navigating the vessel through the restricted waterway.

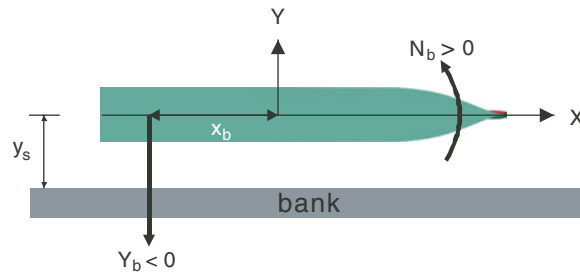


Figure 1. Forces acting on ship when navigating in close proximity to lateral bank.

While the validity of the mathematical models embodied in the Standards for Ship Manoeuvrability International Maritime Organization (IMO) in 2002 is generally accepted for assessing the adequacy of manoeuvrability in deep, unrestricted waters at sea speed, their suitability for predicting the effects of the ship-bank interaction when navigating in narrow waterways is subject to considerable doubt. However, due to prohibitive costs, very few ship trials have been performed in shallow water, and the resulting lack of experimental data seriously limits the ability of existing ship-handling simulators to accurately reproduce the yaw and sway motions experienced by a vessel when operating in close vicinity to a bank (Alexander 2005). Nonetheless, as the rate at which the dimensions of many types of ships continues to outstrip that at which the dimensions of the access channels, rivers and ports frequented by these vessels are enlarged, the need for more realistic prediction methods for enhancing the capabilities of ship-handling simulators is emerging as a major concern in the maritime community (Lataire et al. 2006).

Due to the expense of conducting real-ship experiments under realistic shallow-water conditions, most previous investigations into the bank effect have taken the form of ship model tests performed in a towing tank. Norrbin (1974) investigated the forces acting on a ship in a short dredged channel and found that the bank effect had a significant impact upon the hydrodynamic force coefficient of the vessel. Ch'ng (1991) and Ch'ng and Renilson (1993) showed that the magnitude and direction of the yaw angle and sway force experienced by a vessel operating in restricted water are highly sensitive to variations in the hull form, the vessel speed, the distance to bank, the slope of the bank and the propeller speed for values of the water-depth-to-draught ratio of less than 1.5. Li (2000) conducted a series of experimental trials to investigate the bank effects exerted on three different ship models under extreme shallow water and near-bank conditions. The results showed that at water-depth-to-draught ratios of less than approximately 1.1, the sway force changed from a suction force to a repulsion force and a significant increase occurred in both the sway force and the yaw moment as a result of the significant magnification of the Bernoulli wave effect. Utilizing two bulk carrier models from the MarAd series and the S175 containership, Duffy (2002) performed a series of model scale experiments to clarify the respective effects of the water depth, ship draught, bank height, bank slope and the distance to bank on the resultant sway force and yaw moment. The results of a regression analysis showed that both the sway force and the yaw moment were linearly related to the distance-to-bank parameter. Lataire et al. (2006) performed towing tests in the Towing Tank for Manoeuvres in Shallow Water at the Flanders Hydraulic Research

Centre in Ghent University, Belgium, using three models, namely an 8000 TEU container carrier, a 131,235 m³ LNG carrier and a small tanker. The experiments were aimed predominantly at clarifying the effects of the bank geometry on the magnitude of the bank effects induced on vessels with different hull forms, speeds, propulsion forces, drift angles, distances to bank, and so forth. Overall, the results demonstrated that an inverse correlation existed between the ship-to-bank distance and the magnitudes of the sway force and yaw moment, respectively.

With rapid advances in the speed and computational capabilities of mainstream computers in recent decades, the use of computational fluid dynamics (CFD) simulations as a means of predicting the hydrodynamic forces acting on a vessel under a wide range of environmental and operating conditions has attracted considerable interest in the maritime community. For example, Xiong and Wu (1996) applied the Rankine source method to investigate the hydrodynamic forces acting on the hull of a ship with a free surface effect whilst in restricted water. Ohmori (1998) and Berth et al. (1998) performed Finite Volume Method (FVM) simulations and FLUENT CFD simulations, respectively, based on the Navier-Stokes equation to model the viscous flow field and hydrodynamic characteristics of the ESSO OSAKA oil tanker while advancing and turning in shallow waters. Chen et al. (2002; 2003) utilized the chimera RANS method to examine the problem of ship-to-ship interactions in shallow water and restricted waterways.

In general, the results of the CFD studies discussed above confirm the validity of the CFD approach as a means of obtaining detailed insights into the bank effects acting on vessels operating in restricted water. Accordingly, this study conducts a series of simulations using the commercial FLOW-3D[®] software package to investigate the ship-bank interaction effect for a Post-Panamax container ship advancing at a constant speed in a direction parallel to that of a lateral bank. The simulations focus specifically on the respective effects of the ship speed and distance-to-bank parameter on the time-based variation of the magnitude and direction of the yaw moment and sway force. In addition, the bank effect phenomena are clarified by reference to visualization plots showing the evolution over time of the pressure and velocity distributions in the immediate vicinity of the vessel. Overall, the results presented in this study contribute a further understanding of the bank effect and yield a useful set of guidelines suitable for implementation into ship-handling simulators designed to predict the response of a vessel under near-bank conditions.

2. NAVIER-STOKES EQUATIONS. In the FLOW-3D[®] CFD simulations performed in this study, the motion of the water surrounding the ship is modelled using the Navier-Stokes equations. Given an orthogonal coordinate system, the Navier-Stokes continuity equation has the form

$$\nabla \cdot \vec{V} = 0, \quad (1)$$

while the momentum equation is given by

$$\frac{\partial \vec{V}}{\partial t} + (\vec{V} \nabla) \vec{V} = -\frac{1}{\rho} \nabla p + \nu (\nabla^2 \vec{V}) - g\vec{k}, \quad (2)$$

where \vec{V} denotes the velocity component in the x-, y- or z-direction, respectively, P is the pressure, ρ and ν are the density and viscosity coefficient of the fluid, respectively,

Table 1. Parameters of real ship and KCS 3600 TEU model.

Parameter	Units	Real ship	Ship model
Scale ratio λ	—	1	31.5994
Length between perpendiculars L_{pp}	m	230.0	7.2786
Ship beam B	m	32.2	1.0190
Draught T	m	10.8	0.3418
Displacement force Δ	tons	53330.0	1.6909
Displacement volume	m ³	52030.0	1.6497
Wetted surface S	m ²	9424.0	9.4984
Block coefficient C_B	—	0.6508	0.6508
Longitudinal prismatic coefficient C_P	—	0.6608	0.6608
Transverse metacentric height \overline{GM}	m	7.326	0.2318
L_{pp}/B	—	7.143	7.1430
B/T	—	2.981	2.9810
Gravitational acceleration g	m/s ²	9.81	9.8080
Fluid density ρ	kg/m ³	1025	1025
Centre of mass x	m	111.6	3.53
Centre of mass y	m	0.0	0.0
Centre of mass z	m	5.9	0.187
I_{xx}	kg-m ²	5.69284304e+9	1.8109678e+2
I_{yy}	kg-m ²	7.7933131e+11	2.47507527e+4
I_{zz}	kg-m ²	7.8043431e+11	2.47861275e+4
I_{xy}	kg-m ²	-3.97e+2	1.77e-04
I_{yz}	kg-m ²	1e+2	3.4e-04
I_{zx}	kg-m ²	3.38242495e+10	1.0741759e+3

and g is the gravitational force. Note that in performing the simulations, all the parameters in Equations (1) and (2) other than the ship velocity are assumed to be constant.

3. NUMERICAL SIMULATION PROCEDURE.

3.1. *Establish ship model.* The simulations performed in this study utilize the KRISO (Korea Research Institute of Ships and Ocean Engineering) 3600 TEU Post-Panamax Container Ship (KCS) model. The major parameters and dimensions of both the simulation model and the actual vessel are summarized in Table 1.

3.2. *Establish test velocity.* As shown in Table 1, the real container ship has a length between perpendiculars of $L_{pp} = 230$ m, and the model scaling ratio is given by $\lambda = L_s/L_m = 31.5994$. Assuming the velocity of the real ship to be denoted as V_s , the equivalent ship model velocity, V_m , was computed in accordance with the following procedure.

In general, the Reynolds number, Re , is given by the ratio of the inertia force to the viscous force, i.e.

$$\frac{V^2/L}{\nu V/L^2} = \frac{VL}{\nu} = Re, \quad (3)$$

where V is the characteristic velocity (m/s), L is the characteristic length (m) and ν is the kinematic viscosity (m²/s). Utilizing the Reynolds number as a similarity parameter to ensure the appropriateness of the modelling results, the following

Table 2. Comparison of real ship velocity and KCS 3600 TEU model velocity.

Real ship velocity (knots)	Real ship velocity (m/s)	Froude number (Fr)	Ship model velocity (m/s)
3	1.54	0.03	0.27
6	3.09	0.06	0.55
9	4.63	0.10	0.82
12	6.17	0.13	1.10
15	7.72	0.16	1.37

condition should hold:

$$(Re)_m = (Re)_s \Rightarrow \left(\frac{VL}{\nu}\right)_m = \left(\frac{VL}{\nu}\right)_s \tag{4}$$

Rearranging, it can be shown that

$$V_m = \frac{v_m L_s}{v_s L_m} V_s = \frac{v_m}{v_s} \frac{230}{31.5994} V_s = 31.5994 V_s = \lambda V_s. \tag{5}$$

Furthermore, assuming the Froude number, *Fr*, of the ship model to be equivalent to that of the real ship, it follows that

$$(Fr)_m = (Fr)_s \Rightarrow \left(\frac{V}{\sqrt{gL}}\right)_m = \left(\frac{V}{\sqrt{gL}}\right)_s \tag{6}$$

Rearranging Equation (6) and introducing the ship length parameter values from Table 1, it can be shown that the ship model velocity is given by

$$V_m = \sqrt{\frac{g_m L_m}{g_s L_s}} V_s = \sqrt{\frac{230}{31.5994}} V_s = \sqrt{\frac{1}{31.5994}} V_s = \sqrt{\frac{1}{\lambda}} V_s. \tag{7}$$

Obviously $\sqrt{\frac{1}{\lambda}} V_s \neq \lambda V_s$, and thus the conditions $(Fr)_m = (Fr)_s$ and $(Re)_m = (Re)_s$ can not be satisfied simultaneously. In other words, the model velocity obtained by assuming a similarity of the Reynolds number differs from that obtained by assuming an equivalent Froude number. In a typical ship model experiment, the characteristic Reynolds number is generally of the order of $10^6 \sim 10^7$, while that for a real ship is usually of the order of $10^8 \sim 10^9$ since the viscous force is much lower relative to the developed inertia force. Since the Froude number, *Fr*, and Reynolds number, *Re*, of the real ship cannot be equal to the Reynolds number, *Re*, and Froude number, *Fr*, of the ship model, respectively, it is simplest for the sake of expediency to neglect the viscous force consideration and to calculate the model velocity based on the Froude equivalency condition. (Note that any errors arising as a result of the corresponding inequality of the Reynolds number can be corrected at a later date based upon experience.) Table 2 compares the real ship velocities and simulation velocities considered in the present study. As shown, the real ship velocities are assumed to be 3, 6, 9, 12 and 15 knots, respectively, corresponding to velocities of 1.54 m/s, 3.09 m/s, 4.63 m/s, 6.17 m/s, and 7.72 m/s, respectively. The equivalent Froude numbers are 0.03, 0.06, 0.10, 0.13 and 0.16, respectively, and thus the ship model velocities are determined to be 0.27 m/s, 0.55 m/s, 0.82 m/s, 1.10 m/s, and 1.37 m/s, respectively.

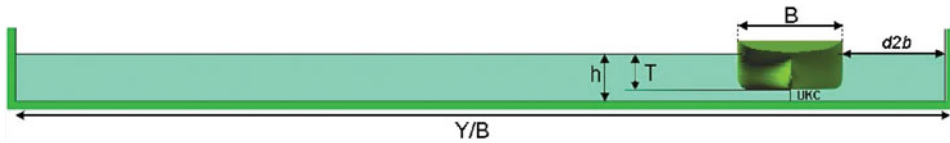


Figure 2. Cross-sectional view of numerical waterway model.

3.3. *Establish numerical model of waterway.* Figure 2 presents a schematic illustration showing the cross-section of the waterway model used in the CFD simulations. Note that in this figure, h is the water depth, T is the draught of the ship model, B is the beam of the ship model, UKC is the under keel clearance, $d2b$ is the distance to bank, and Y/B is the width of the waterway. In general, the correlation between the draught of a ship, the under keel clearance and the water depth is expressed by the ratio h/T (ITTC 2002) and generally varies in the range 1.1 ~ 1.5 for most large ports (Ch'ng 1991; Ch'ng and Renilson 1993; Li 2000). In the present simulations, the water depth is specified as 14.2 m; corresponding to the low-tide depth of the navigation channel in Kaoshiung port in southern Taiwan. As shown in Table 1, the draught of the real Post-Panamax container ship is 10.8 m, and thus the water-depth-to-draught ratio has a value of $h/T=1.31$. To prevent the accuracy of the simulation results for the ship-bank interactions from being affected by the waves reflected from the far bank, the width of the waterway model was specified as eight times the beam of the ship in accordance with the recommendations of the International Towing Tank Conference (ITTC, 2005). Moreover, the length of the waterway was specified as $11B$, $14B$, $17B$, $19B$ or $22B$ for ship model velocities of 0.27m/s, 0.55m/s, 0.82m/s, 1.10m/s and 1.37m/s, respectively. Following a comprehensive grid-dependency test, it was determined that the optimal waterway model comprised a total of approximately 3 million individual grids.

The simulations performed in this study solve the ship-fluid coupled motion equation (Wei 2005) and utilize two orthogonal coordinate systems, namely a body-fixed system and an earth-fixed system (Baha 2000). As shown in Figure 3, the body-fixed system ($x'y'z'$) is attached to the ship model, while the earth-fixed system ($x y z$) is attached to the waterway model. In the simulations, an assumption is made that at time $t=0$, the ship is located at the origin of the waterway framework with the ($x'y'z'$) axes of the ship coordinate system parallel to the corresponding axes of the waterway model. As time elapses, the ship model advances at the specified velocity along the x -axis (i.e. along a direction heading of 090°) and the velocity flow field and pressure distribution in the immediate vicinity of the ship are computed at each time step. As the ship advances, it performs a three degree-of-freedom (3-DOF) motion relative to the (x, y, z) axes of the waterway model, namely “surge”, i.e. a displacement of the ship along the x -axis, “sway”, i.e. a displacement of the ship along the y -axis, and “heave”, i.e. a displacement of the ship along the z -axis. The ship simultaneously performs a 3-DOF motion about its own coordinate framework, namely “roll”, i.e. a rotation about the x' -axis, “pitch”, i.e. a rotation about the y' -axis, and “yaw”, i.e. a rotation about the z' -axis. Thus, the motion of the ship model has potentially six degrees of freedom (6-DOF).

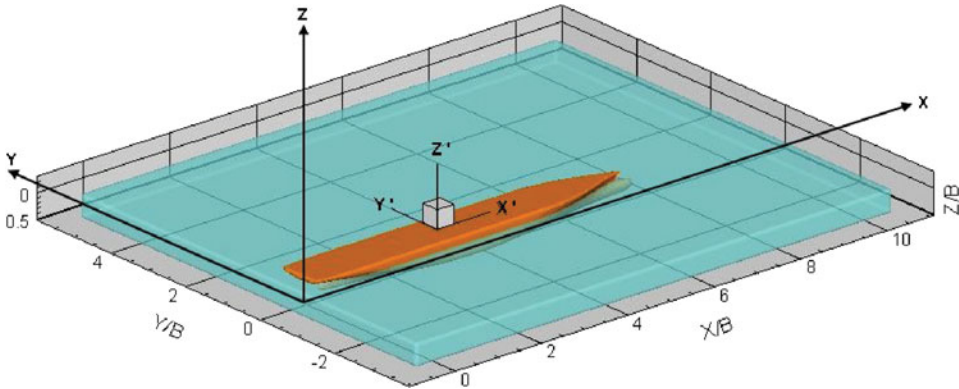


Figure 3. Schematic view of numerical waterway model.

4. RESULTS AND DISCUSSION.

4.1. *Validation of simulation model.* Prior to performing the bank effect simulations, the validity of the FLOW-3D[®] simulation model was confirmed by computing the hydrodynamic resistance acting on a small boat with a length of 3.0 m, a beam of 0.8 m, a draught of 0.2 m and a mass of 118.2 kg as it travelled along the x -axis of the waterway model. The mass centre inertia tensor of the boat is given by

$$I = \begin{bmatrix} 6.7 & 0.0 & 0.0 \\ 0.0 & 93.0 & 0.0 \\ 0.0 & 0.0 & 96.7 \end{bmatrix} (\text{m}^2 \cdot \text{kg}) \quad (8)$$

In the validation simulations, the calculation area comprised a total of 156,388 grids and the solution was obtained using the implicit Successive Over-Relaxation (SOR) scheme with the FLOW-3D[®] Renormalized Group (RNG) turbulence model and General Moving Objects (GMO) model. The simulations considered boat speeds of 5.04 m/s, 5.88 m/s, 6.72 m/s, and 7.98 m/s, respectively, and had a duration of $t = 4\text{ s}$ in every case. The calculated values of the hydrodynamic resistance acting on the boat at each speed are summarized in Table 3. Note that the resistance values presented for speeds of 5.04 m/s, 5.88 m/s and 6.72 m/s, respectively, denote the average value obtained over the last 1 second of the simulation, while that presented for a velocity of 7.98 m/s is the average value computed over the interval $t = 2.2 \sim 4.0\text{ s}$. For comparison purposes, the table also presents the resistance values reported by Azimut Yachts for a vessel of a similar size. It is observed that a good agreement exists between the two sets of results at each value of the boat speed, and thus the basic validity of the simulation model is confirmed.

4.2. *Analysis of ship trajectory.* The simulations commenced by modelling the trajectory of the KCS model over a duration of 12 seconds as it advanced in the eastward direction at a constant speed of 0.27 m/s, 0.55 m/s, 0.82 m/s, 1.10 m/s and 1.37 m/s, respectively. Figure 4 illustrates the trajectories of the KCS model when advancing at a speed of 0.82 m/s at various distances from the bank. Note that in each case, the trajectories are obtained simply by overlaying the positions of the boat after elapsed times of $t = 0\text{ s}$, $t = 2\text{ s}$, $t = 4\text{ s}$, $t = 6\text{ s}$, $t = 8\text{ s}$, $t = 10\text{ s}$, and $t = 12\text{ s}$, respectively.

Table 3. Comparison of FLOW-3D[®] hydrodynamic resistance calculations and shipyard resistance measurements (Wei 2006)

Upstream velocity (m/s)	5.04	5.88	6.72	7.98
Calculated resistance (N)	169.0	187.1	185.3	210.2
Measured resistance (N)*	171.4	178.2	188.2	217.1
Error (%)	1.4	5.0	1.5	3.2

* Data reproduced courtesy of Azimut Yachts.

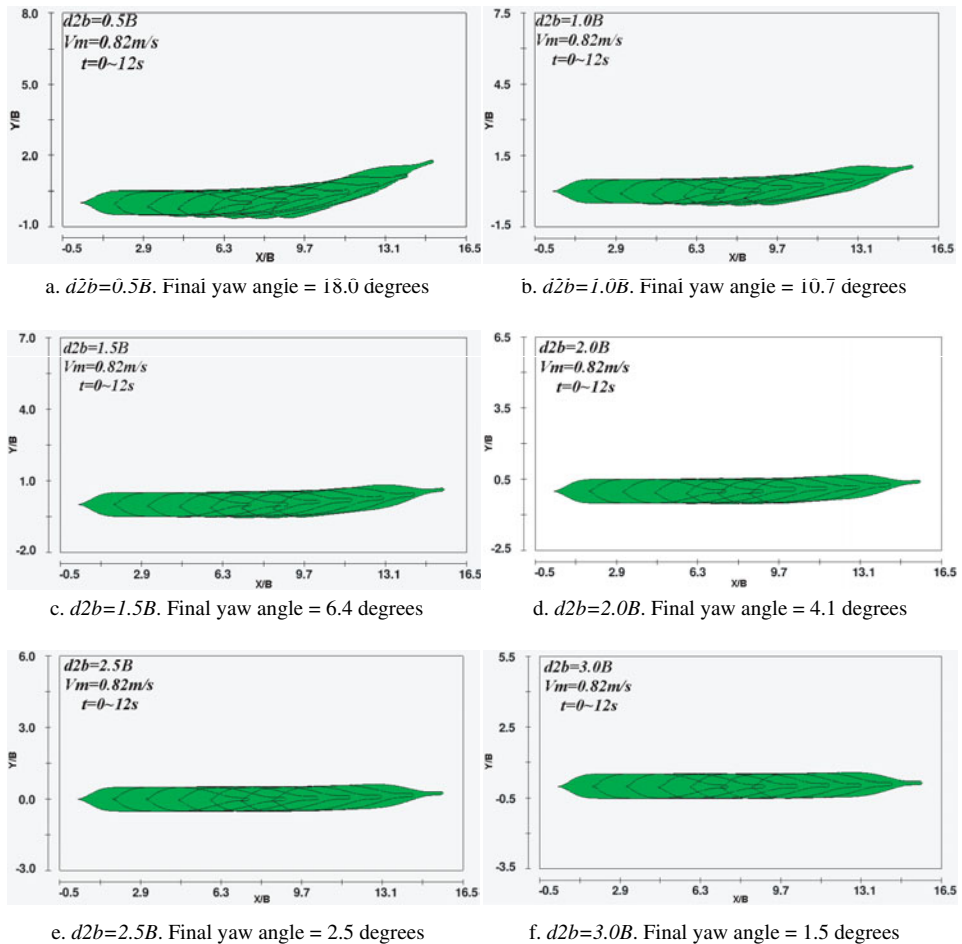


Figure 4. Ship trajectories whilst navigating at $V_m=0.82$ m/s with $d2b=0.5 \sim 3.0B$.

In every sub-figure, the x-axis (X/B) indicates the displacement of the ship model in the eastward direction, while the y-axis (Y/B) represents the perpendicular distance between the mass centre of the ship model and the bank. Meanwhile, the caption beneath each sub-figure indicates the yaw angle of the ship model upon completion of the simulation (i.e. $t=12$ s). The simulation results clearly show that for a constant ship speed, the yaw angle increases as the distance between the ship and the bank

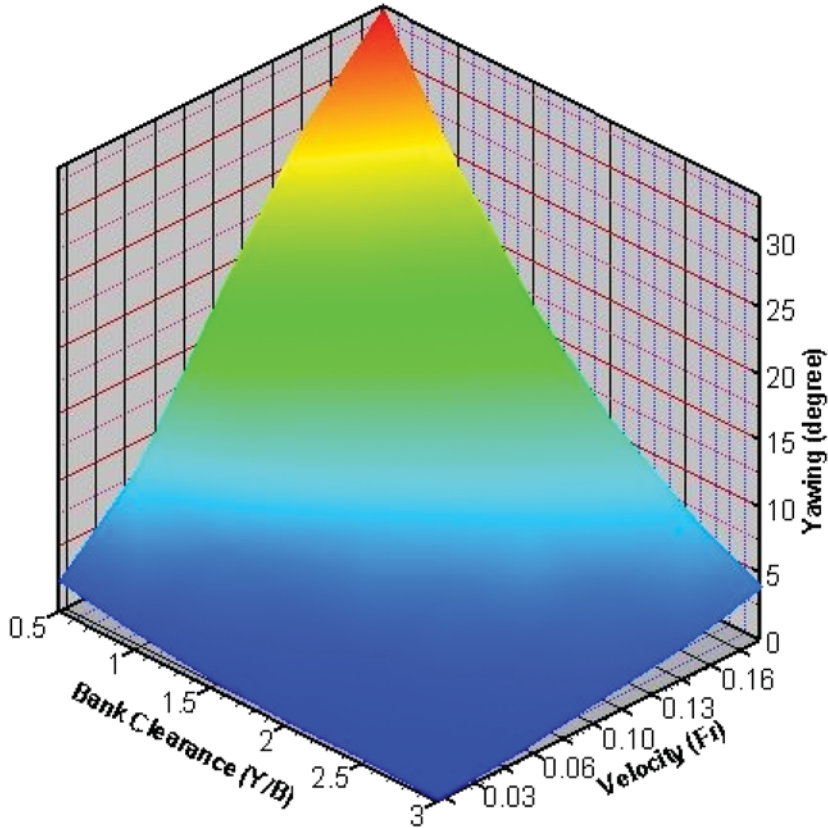


Figure 5. Correlation between distance to bank, ship speed and yaw angle.

reduces. From inspection, the final yaw angle for an initial ship-to-bank distance of 0.5B is determined to be 12 times higher than that of the final yaw angle for an initial ship-to-bank distance of 3.0B.

4.3. *Analysis of yaw angle and yaw velocity.* Figure 5 illustrates the correlation between the distance to bank, the ship speed and the yaw degree. The results confirm that for a constant ship velocity, the yaw angle increases significantly with a reducing distance to bank. In addition, it is observed that the sensitivity of the yaw angle to the distance-to-bank parameter is particularly pronounced at higher values of the ship speed. The results also show that for a given value of the distance-to-bank parameter, the yaw angle increases with an increasing velocity; particularly at lower values of the ship-to-bank distance.

Since the ship model potentially performs a 6-DOF motion, the bow may rotate about the z-axis at the same time as the ship advances along the x-axis. According to the right-hand law, a positive value of the angular yaw velocity indicates a counter-clockwise rotation of the bow, i.e. the bow moves in the port direction and the heading angle reduces. Conversely, a negative value of the angular yaw velocity indicates that the bow rotates in the clockwise direction, i.e. the bow moves in the starboard direction and the heading angle increases. Figures 6(a) and 6(b) illustrate

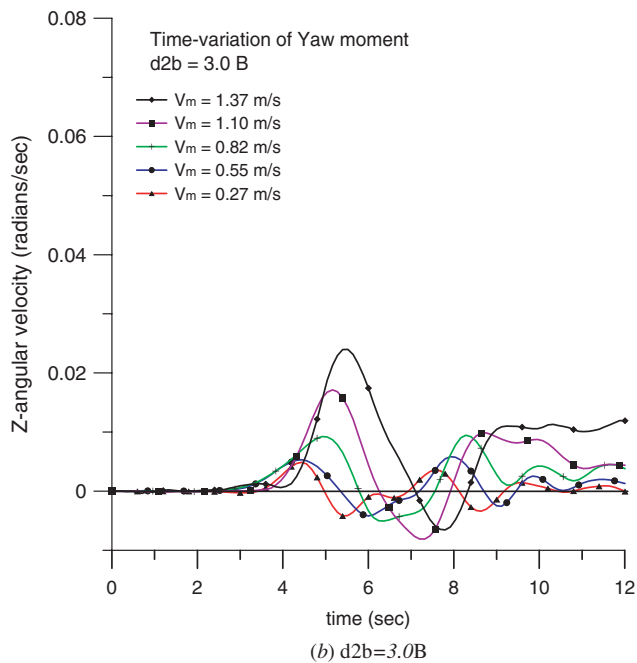
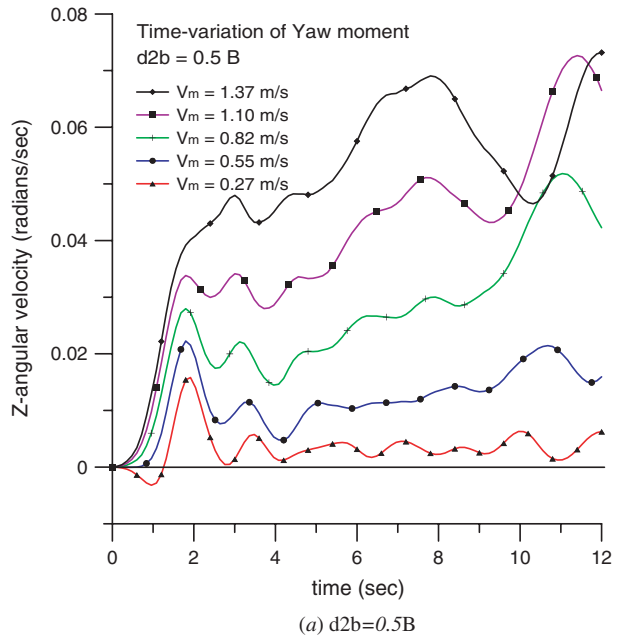


Figure 6. Time-based variation of yaw moment as function of ship speed for: (a) $d2b=0.5B$ and (b) $d2b=3.0B$.

the time-based variation of the yaw velocity as a function of the ship model speed for distance-to-bank values of $0.5B$ and $3.0B$, respectively. Figure 6(a) shows that at a low value of the ship-to-bank distance, the yaw velocity has a consistently positive

value at virtually all values of the ship speed, which indicates that the bow rotates in the counterclockwise direction, i.e. away from the bank. Furthermore, it can be seen that the magnitude of the yaw velocity is significantly dependent upon the ship speed, and increases with an increasing velocity. For the case of a higher ship-to-bank distance, the results presented in Figure 6(b) indicate that for a constant velocity, the bow of the ship tends to oscillate between the port and starboard directions as the ship advances. Furthermore, it is evident that the magnitude of the yaw velocity is relatively insensitive to the ship speed. Overall, therefore, the results suggest that the bank effect diminishes as the distance between the ship and the bank increases.

4.4. *Analysis of sway force.* Figures 7(a) and 7(b) illustrate the time-based variation of the sway force as a function of the ship speed at distance-to-bank values of $0.5B$ and $3.0B$, respectively. Comparing the two figures, it is evident that the sway force is dominated by the distance-to-bank parameter, whereas the ship speed has a relatively lesser effect. Furthermore, it is seen that the individual sway force profiles have a relatively uniform oscillatory characteristic with a period of approximately 2 seconds. An increasing value of the sway force indicates that the flow field between the ship and the bank forces the ship toward the centre of the channel, whilst a decreasing value of the sway force indicates that the flow field pulls the ship toward the bank. The two figures show that the bank effect is first manifested after an elapsed simulation time of approximately 3 seconds, i.e. the sway force adopts a negative value, which indicates that the stern of the ship approaches the bank as a result of the yaw rotation of the bow in the port direction (see Figure 6).

Figure 8 illustrates the correlation between the distance to bank, the ship speed and the sway force. In general, the results show that for a constant value of the ship-to-bank distance, the sway force increases with an increasing velocity. The sensitivity of the sway force to variations in the ship speed is particularly pronounced at low values of the ship-to-bank distance. Meanwhile, for a constant value of the ship speed, the sway force increases with a reducing ship-to-bank distance. The sensitivity of the sway force to changes in the ship-to-bank distance is particularly apparent at higher values of the ship speed.

4.5. *Analysis of flow field pressure distribution at $V_m = 0.82 \text{ m/s}$.* Figures 9(a~b) and 9(c~d) illustrate the time-based evolution of the pressure distribution on the x - y plane located at a depth of $-0.06 (Z/B)$ for distance-to-bank values of $0.5B$ and $3.0B$, respectively. Note that the ship speed is 0.82 m/s in both cases. Comparing the two figures, it is observed that the pressure distribution around the ship model is far more uniform in the case of the higher ship-to-bank distance, and thus no more than a minor yawing of the bow takes place. However, in the case of the low ship-to-bank distance, it can be seen that a significant low-pressure region is formed on either side of the ship in the mid-length position after a simulation time of around $t = 3 \text{ s}$. As further time elapses, the low-pressure region on the port side of the ship contracts, while that on the starboard side enlarges and moves toward the bow, prompting the bow to rotate toward the middle of the channel.

4.6. *Analysis of stern vortex flow.* Figure 10 illustrates the evolution of the flow field at the stern of the ship model at elapsed simulation times of $t = 3 \text{ s}$, $t = 6 \text{ s}$, $t = 9 \text{ s}$ and $t = 12 \text{ s}$, respectively, corresponding to x -axis displacements of $X/B = 2.6$, 4.5 , 6.5 and 8.3 , respectively. Note that in every case, the distance-to-bank parameter has a

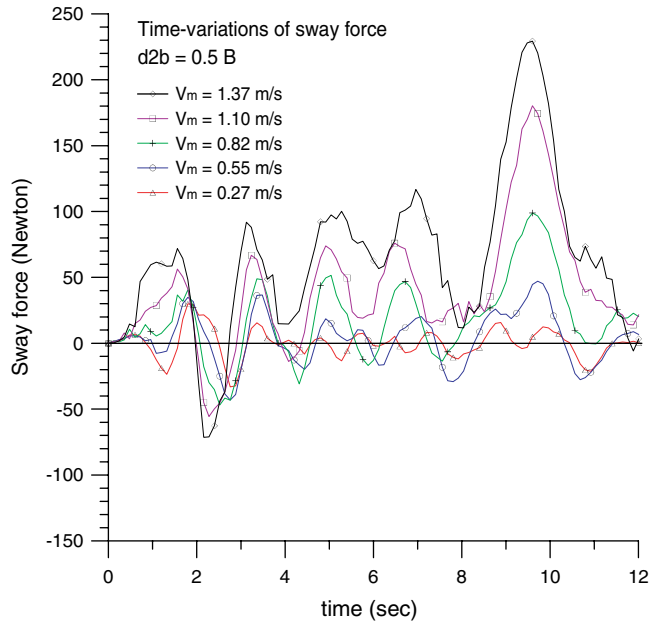
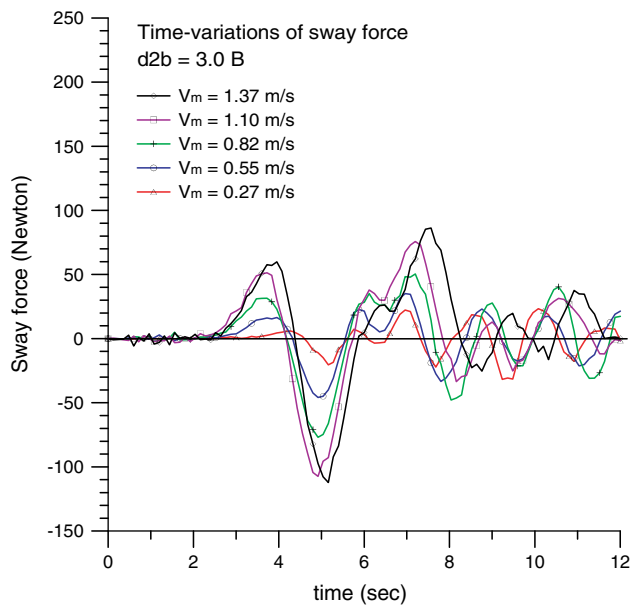
(a) $d2b=0.5B$ (b) $d2b=3.0B$

Figure 7. Time-based variation of sway force as function of ship speed for: (a) $d2b=0.5B$ and (b) $d2b=3.0B$.

value of $0.5B$ and the ship advances at a velocity of 0.82 m/s. The results reveal the formation of a significant vortex structure on the port side of the stern, which drives the stern toward the bank, resulting in a yaw motion of the bow.

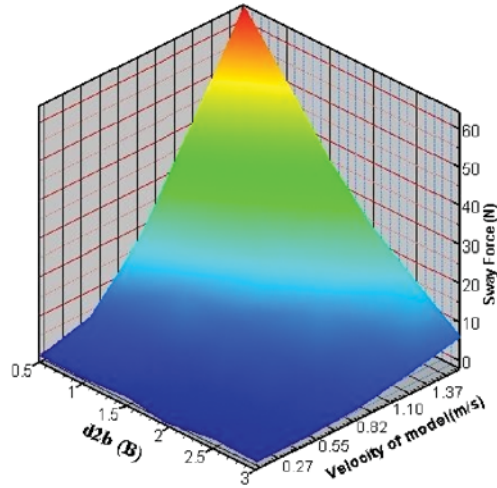


Figure 8. Correlation between distance to bank, ship speed and sway force.

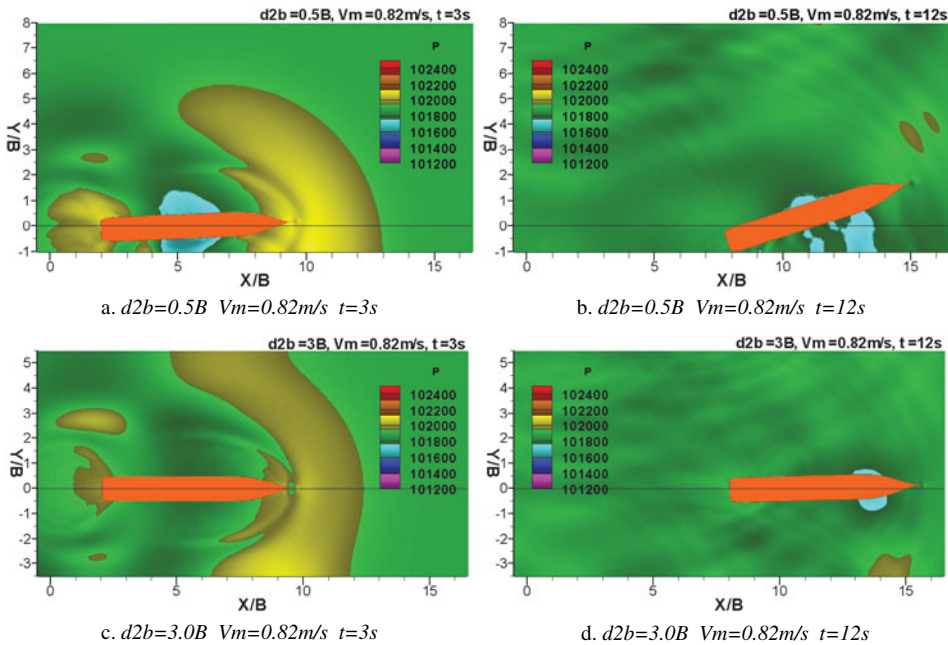


Figure 9. Time-based evolution of pressure field distribution for $d2B=0.5B$ and $d2b=3.0B$ at constant $Vm=0.82\text{ m/s}$.

5. CONCLUSION. The FLOW-3D[®] CFD simulation results presented in this study for the bank-effects acting on a 3600 TEU Post-Panamax container ship with a water-depth-to-draught ratio of approximately 1:3 support the following major conclusions:

- For a given value of the ship speed, the yaw angle and sway force increase with a reducing distance to bank.

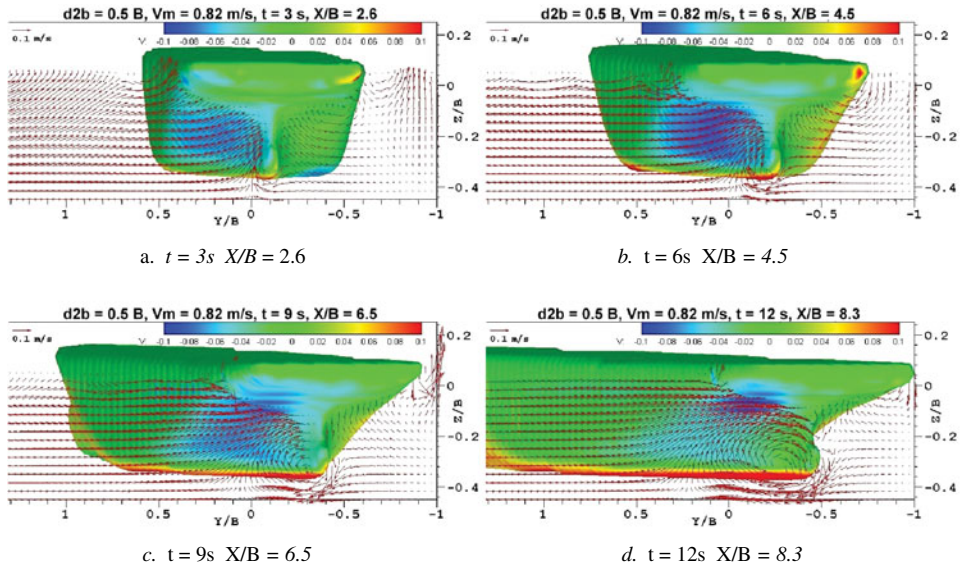


Figure 10. Time-based evolution of stern vortex flow field for $d2b=0.5B$ and $Vm=0.82\text{ m/s}$.

- For a given value of the distance-to-bank parameter, the yaw angle and sway force increase with an increasing ship speed.
- For a low ship model velocity of $Vm=0.27\text{ m/s}$, the yaw angle at a distance-to-bank value of $0.5B$ is around 24 times higher than that obtained at the same velocity for a distance-to-bank value of $3.0B$. Thus, the results indicate that the bank effects must be taken into consideration when performing ship handling operations in very close proximity to a bank even if the vessel is moving at a very low speed.
- Irrespective of the distance of the vessel from the bank, the bank effects increase significantly when the ship model velocity exceeds a value of $Vm=0.55\text{ m/s}$. In other words, the results suggest that ship manoeuvres in restricted waters should take place at a speed carefully selected to minimize the bank effect.

Overall, the results presented in this study confirm the validity of the CFD simulation approach for modelling the bank effect phenomenon and provide useful guidelines for ship handling manoeuvres involving meeting, passing, docking, tugboat operations, and so forth in restricted water.

ACKNOWLEDGMENTS

The support by the National Science Council, Taiwan under the grant no. 96-2221-E-022-014 for the work is gratefully acknowledged.

REFERENCES

- Alexander C. Landsburg (2005), Critical Needs for Ship Manoeuvrability: Lessons From the Houston Ship Channel Full-Scale Manoeuvring Trials, *Marine Technology*, Volume 42, pp. 11–20.
- Baha M. Suleiman (2000), Identification of Finite-Degree-of-Freedom Models for Ship Motions, Virginia Polytechnic Institute and State University.

- Berth, F., Bigot, E. and Laurens, J. M., (1998), Numerical simulations of the ESSO Osaka, International Symposium and Workshop on Forces Acting on a Manoeuvring Vessel, Val de Reuil, France.
- Chen, H. C., Lin, W. M., and Hwang, W. Y. (2002), Validation and Application of Chimera RANS Method for Ship-Ship Interactions in Shallow water and Restricted Waterway, 24th Symposium on Naval Hydrodynamics, Fukuoka, Japan, 8–13 July.
- Chen, H. C., Lin, W. M., Liut, D. A., and Hwang, W. Y. (2003), An Advanced Flow Computation Method for Ship-Ship Dynamic Interactions in Shallow and Restricted Waterway, MARSIM'03, Kawakawa, Japan.
- Ch'ng, P. W. (1991), An Investigation into the Influence of Bank Effect on Ship Manoeuvring and Its Mathematics Modelling for a Ship-Handling Simulator, ME. Thesis, School of Mechanical and Manufacturing Engineering, the University of New South Wales, Australia.
- Ch'ng, P. W., Renilson, L. J. (1993), A method of calculating the ship bank interaction forces and moments in restricted water, International Shipbuilding Progress.
- Duffy, J. T. (2002), The Effect of Channel Geometry on Ship Operation in a Port, Presented at 30th PIANC-AIPCN Congress, Sydney, September 2002.
- ITTC (2002), ITTC symbols and terminology list, version 2002, ITTC.
- ITTC (2005), The Maneuvering Committee, Final Report and Recommendations to the 24th ITTC.
- Lataire, E., Vantorre, M., Laforce, E., Eloit, K., Delefortrie, G. (2006), Navigation in confined waters: influence of bank characteristics on ship-bank interaction.
- Li, D-Q., (2000), Experiments on Bank Effects under Extreme Conditions, SSPA Report No. 113, Goteborg, Sweden.
- Norrbin, N. H. (1974), Bank Effects on a Ship Moving Through a Short Dredged Channel, Proceedings 10th Symposium on Naval Hydrodynamics, pp. 71–88.
- Ohmori, T. (1998), A study on hydrodynamic characteristics of a maneuvering ship in shallow water by a Finite-Volume method, International Symposium and Workshop on forces acting on a maneuvering vessel.
- Wei Gengsheng (2005), A fixed-mesh method for general moving objects, Flow Science, Inc.
- Wei Gengsheng (2006), An implicit method to solve problems of rigid body motion coupled with fluid flow, Flow Science, Inc.
- Xiong, X. M., Wu, X. H., (1996), A study on maneuvering hydrodynamic forces acting on 3d ship-hulls with free surface effect in restricted water, International Shipbuilding Progress, Vol. 43, pp. 48–69.